ABraytCSPfuture

Air-Brayton Cycle Concentrated Solar Power future plants via redox oxides-based structured thermochemical heat exchangers / thermal boosters

Deliverable D3.1

Properties of structured ceramic model specimens as a function of temperature

Dissemination Level: Public

WP3 Preparation of lab-scale redox oxides porous structured test specimens and application-specific testing

Date: 21.02.2025

Disclaimer

The work described in this document has been conducted within the ABraytCSPfuture project that is co-funded by the European Union. Views and opinions expressed herein are however those of the author(s) only and do not necessarily reflect those of the European Union or of the granting authority, European Climate, Infrastructure and Environment Executive Agency (CINEA). Neither the European Union nor the granting authority can be held responsible for them.

Grant Agreement Number: 101084569 Acronym: ABraytCSPfuture				
Full Title	**A**ir-**Brayt**on Cycle **C**oncentrated **S**olar **P**ower **future** plants via redox oxides-based structured thermochemical heat exchangers/thermal boosters			
Call Topic Identifier:	HORIZON-CL5-2021-D3-03			
Funding Scheme	HORIZON EUROPE, RIA – Research and Innovation Actions			
Project start date:	01.11.2022			
Project duration:	48 months			
Project URL	https://www.abraytcspfuture.eu/			
EU Project Officer	Clara Astudillo Llorente			
Project Coordinator	DLR – German Aerospace Center			
Deliverable	D3.1 – Properties of structured ceramic model specimens as a function of temperature			
Date of Delivery	Contractual	31.01.2025	Actual	21.02.2025
Nature	Report			
Dissemination Level	Public			
Lead Beneficiary	CERTH – Centre for Research and Technology Hellas			

Document History

Version	**Issue Date**	**Change History**	**Authors**	**Organisation**
1.0	26.01.2025	Document drafted	George Karagiannakis, Chrysa Pagkoura	CERTH
1.1	15.02.2025	Updated with final partner feedback	Christos Agrafiotis, David Vellas, Mathias Pein, Asmaa Eltayeb, Raisa dos Santos Santana	DLR
1.2	20.02.2025	Final Review	Javier Baigorri Martinez	CENER

About the Project

ABraytCSPfuture sets forth an innovative, carbon-neutral way for implementing the highly efficient air-Brayton gas turbine power generation cycles into future air-operated Concentrated Solar Power (CSP) plants. Air-Brayton cycles are used in traditional power plants where, however, involve fossil fuels combustion via pressurized air. *ABraytCSPfuture's* carbon-neutral approach aims at achieving higher solar-to-electricity efficiencies, vital for competitiveness of CSP and non-reachable by either PVs or molten salts and thermal oils, increasing in parallel significantly the plants' storage capability. The project will develop and demonstrate a first-of-its-kind compact, dual-bed thermochemical reactor/heat exchanger unit that will transfer heat from a non-pressurised air stream to a pressurised one, while also operating as a thermal booster, raising the temperature of the pressurized stream to the level required for Brayton cycles. Furthermore, the volumetric solar energy storage density of air-operated CSP plants will be significantly increased by rendering their current sensible-only regenerative storage systems to hybrid sensible-thermochemical storage ones within the same storage volume. Both these functionalities will be materialized by thermochemical reactor/heat exchanger units comprised of non-moving, flow-through porous ceramic structures (honeycombs or foams) based on earth-abundant, cost-efficient, non-toxic oxide materials and exploiting reversible reduction/oxidation reactions of such oxides in direct contact with air, accompanied by significant endothermic/exothermic heat effects. The proposed technology is set forth by an interdisciplinary partnership spanning the entire CSP value chain, comprised of leading research centres, universities, innovative SMEs and large enterprises, including ancillary services providers and technology end-users.

Deutsches Zentrum fuer Luft- und Raumfahrt e.V., **DLR**	DE	DLR
Centre for Research & Technology Hellas, **CERTH**	EL	CERTH CENTRE FOR RESEARCH & TECHNOLOGY HELLAS
University of Twente, **UT**	NL	UNIVERSITY OF TWENTE.
Fundación CENER, **CENER**	ES	CENER NATIONAL RENEWABLE ENERGY CENTRE ADItech
Fundación TEKNIKER, **TEKN**	ES	Tekniker
Fraunhofer Gesellschaft zur Foerderung der angewandten Forschung e.V., **FHG (IWKS)**	DE	Fraunhofer IWKS
OPRA Turbines, **OPRA**	NL	Destinus
KRAFTBLOCK GmbH, **KB**	DE	KRAFT BLOCK
LANDSON Emission Technologies A/S, **LET**	DK	landson
COBRA Instalaciones y Servicios S.A., **COBRA**	ES	cobra

Table of Contents

This deliverable is part of a project that has received funding from the European Union's Horizon Europe research and innovation programme under grant agreement no 101084569

Executive Summary

This document relates to the main aspects and methodologies followed to prepare all-redox perovskite lab-scale structured bodies (i.e. foam-like by sacrificial polyurethane/PU template/matrices and honeycombs by extrusion). The main compositions reported here are $CaMnO_3$ (CMO), $Ca_{0.90}Sr_{0.10}MnO_3$ (CS10MO) and 3 Fe-doped compositions in the Mn-site of CS10MO. The deliverable also refers to physicochemical characterization, which provides insights on the main properties that define textural and preliminary thermochemical properties of the structures in question. The redox thermochemical performance is addressed in detail and under more realistic and multi-cyclic protocols in deliverable D3.2. The methods followed were successful and, to the knowledge of the consortium by the time of submission of this document, this is the first time that such structures are reported to have been successfully manufactured. In the case of extrusion, low-cost, sensible-only honeycomb structures of a specific geometry were also prepared successfully. Regarding scaling-up perspectives of the small-scale structures reported here, please refer to deliverable D3.3.

Changes with respect to the DoA

There are no notable changes referring to the DoA and thus the timely preparation of the present deliverable and implementation of the workplan of WP3, until submission of this deliverable, have not been affected.

1. Introduction

The present deliverable refers to the measured properties of developed small-scale specimens (porous foams and honeycombs) to optimize manufacturing conditions for production of structures with optimal heat transfer and thermomechanical stability characteristics. The results reported here refer to Tasks 3.1 and 3.2 of WP3.

The aspects addressed in this document directly relate to measurements/analyses and parametric studies to achieve small-scale structured specimens that combine in-principle very good heat transfer characteristics and sufficient robustness. Optimization is not thoroughly pursued as past experience has clearly indicated that despite scaling-up of the manufacturing process must use the relevant findings from small-scale studies as starting point, substantial modifications may be required in practice to tackle the challenges of achieving acceptable structures at larger sizes. Thus, this optimization process will be more actively pursued during scaled-up shaping in WP5. To obtain the complete picture and conclude with the choice of redox oxides formulations/structures for the proof-of-concept scale unit (see D3.3), one should actually combine the content and main results from this deliverable with the ones reported in deliverable D3.2.

2. Overview of materials of choice

The main list of powder formulations considered for the lab-scale shaping activities, which will continue until M42, is the one qualified by the WP2 studies and included in deliverable D2.4. This list has been extended by the addition of 3 extra powders based on findings of WP2 after the submission of D2.4, which are described below. These are 2 redox compositions and 1 suitable for sensible-only heat storage compositions. The latter was obtained from steel industry by-products and was provided by KB. In addition, the $SrFeO_3$ stoichiometry was eventually removed from the list due to its low energy density.

Several features were taken into account in order to assemble this list of selected material compositions. To conform to the target of using exclusively earth-abundant compounds, the CMO-based reference compositions were doped with iron (Fe) at the B-site (replacing some of the Mn). Another crucial feature is the absence of the orthorombic-to-cubic transformation, which, although reversible, is considered detrimental to the long-term integrity and performance of structured objects due to the associated lattice expansion/contraction taking place during cyclic heating/cooling, which induces thermochemical stresses on the structure. The existence or absence of this transformation can be verified simultaneously with the measurements of the heat capacity of powder compositions as a function of temperature; heat capacity is another essential property, since the higher it is, the more effective a structured object is at storing sensible heat. Another relevant feature is the reversibility and magnitude of the change in the dimensions of the structured objects due to combined thermal-thermochemical expansion/contraction. This magnitude will affect the design of the dual-bed unit in WP5.

Figure 1 shows the heat capacity measurements of the Calcium manganite ($CaMnO_3$) and certain Sr-doped compositions, of compositions in which Ca is not doped with Sr but Mn is doped with varying amounts of Fe, and variations of the stoichiometry $Ca_{0.90}Sr_{0.10}MnO_3$ (CS10MO) wherein Mn is also doped with varying amounts of Fe. From the graph it is evident that Fe-doping on the B-site seems to affect the orthorhombic-to-cubic transformation in a similar way as Sr-doping on the A-site: compositions without Sr but with Fe stop to exhibit this transformation when Fe exceeds a certain value, ca. 10 at %. As expected, compositions that include both Sr and Fe beyond a critical amount, ca. 10 at% for either one, do not exhibit this transformation at all. Further addition of Sr and Fe seems to slightly decrease the heat capacity.

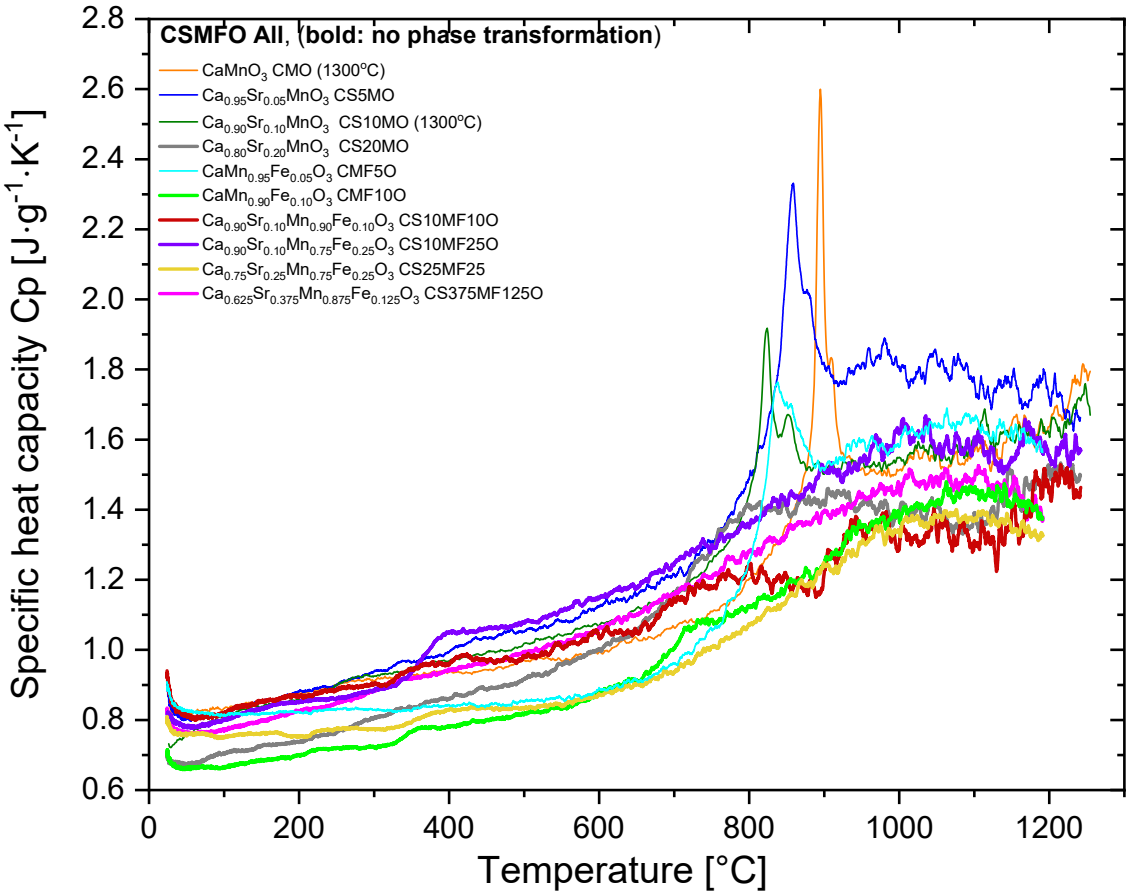

Figure 1: Measured specific heat capacity (Cp) values as a function of temperature for the 3 reference compositions and those further doped with iron in the B-site. The peak shows the occurrence of the orthorombic-to-cubic tranformation.

Dilatometry experiments were performed on prism-shaped specimens sectioned from sintered bars made of selected Fe-doped compositions under the same protocol with older such measurements on CMO, CS5MO and CS10MO specimens [1, 2] in a contactless optical dilatometer. The experiments were carried out under air atmosphere and an identical 5 cycle heating/cooling protocol between 300-1100°C. The results, in comparison to the prior ones, are shown in Figure 2 in the terms of relative length change ($\Delta L/Lo$) and coefficient of thermal expansion (CTE) over the 5 heating and cooling cycles.

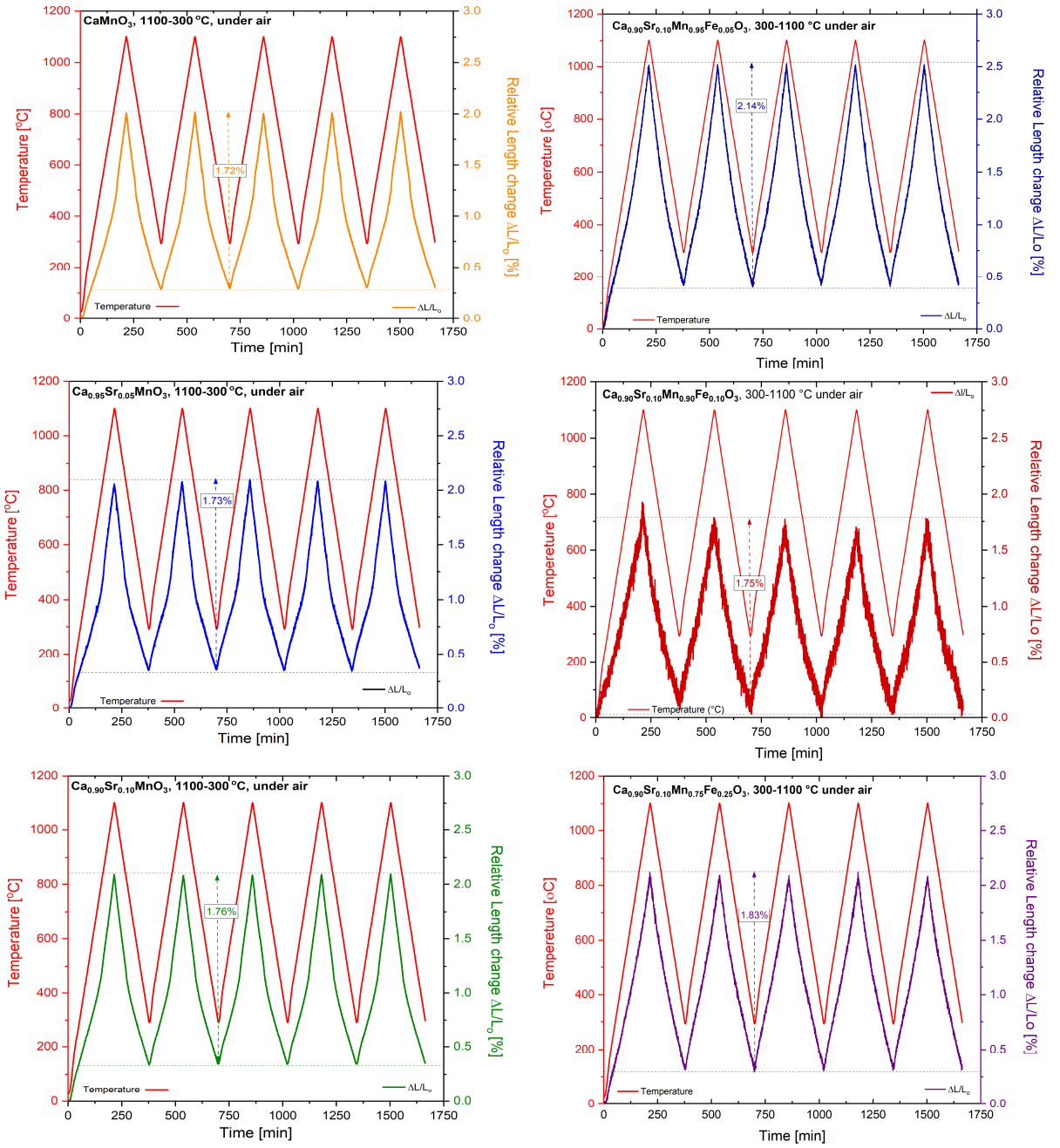

Figure 2: Thermal expansion of CMO-based compositions measured by optical dilatometry in air and cycled between 300-1100°C: left column $CaMnO_3$ (CMO), $Ca_{0.90}Sr_{0.10}MnO_3$ (CS5MO) and $Ca_{0.90}Sr_{0.10}MnO_3$ (CS10MO); right column: variations of the CS10MO) composition doped with increasing amount of Fe in the B-site, (CS10MF5O, CS10MF10O, CS25MF75O).

The CTE is calculated as (L-Lo)/(T-To) with Lo corresponds to the initial specimen length at ambient temperature To. Two out of the three Fe-containing compositions, namely $Ca_{0.90}Sr_{0.10}Mn_{0.95}Fe_{0.05}O_3$ (CS10MF5O) and $Ca_{0.90}Sr_{0.10}Mn_{0.75}Fe_{0.25}O_3$, (CS25MF75O) seem to exhibit a reversible length change, the magnitude of which decreases with increasing Fe content. The one with intermediate Fe doping, $Ca_{0.90}Sr_{0.10}Mn_{0.90}Fe_{0.10}O_3$ (CS10MF10O) exhibits fluctuations of this length change from cycle to cycle. Table 1 and Table 2, summarize the results of these two sets of measurements on the list of 9 compositions in powder form qualified for further

experimental consideration in WP2 and WP3. Out of the 9 compositions, the four new ones are indicated in bold. Where applicable (e.g. refined Cp values as measured from CERTH and DLR after submission of D2.4), additional updated information was included.

For more information and explanations relating to the preparation of the powders and their main attributes, thermal properties measurements, methodology of evaluation/ qualification/characterization etc., the reader should refer to deliverables D2.2 – D2.4. All 9 of them have been fed to WP3 for consideration; i.e. tests on their suitability for shaping into structures, redox/ thermochemical/ thermomechanical/ physicochemical evaluation and characterization etc. Calcium manganite ($CaMnO_3$) and certain Sr-doped compositions derived from it are the primary materials of choice at the time of preparation of this deliverable (M28).

Composition		**Transitions♣**	**δ♦**	**Heat Capacity***	**$\Delta L/L_o$ (%)**	**Reversible ΔL**
CMO		Yes	< 0.19	1.21 J/g/K	1.72	Yes
CS5MO		Yes	< 0.20	1.27 J/g/K	1.73	Yes
CS10SMO		No	< 0.19	1.39 J/g/K	1.76	Yes
CS10MF5O		No	N/M	N/M	2.14	Yes
CS10MF10O		No	N/M	1.12 J/g/K	1.75	No
CS10MF25O		No	< 0.22	1.27 J/g/K	1.83	Yes
Non-redox	A4	N/A	N/A	1.22 J/g/K	N/M	N/M
	BM/B	N/A	N/A	1.04 J/g/K	N/M	N/M
	T12	N/A	N/A	1.10 J/g/K	N/M	N/M

♣: *Reversible structural transitions from orthorombic-to-cubic*

♦*: Non-stoichiometry parameter*

***: average value in the 300-1100°C targeted operating temperature range of the project*

Table 1: Summary of existence of phase transitions, non-stoichiometry parameter, average heat capacity and dimensional changes of perovskite compositions.

Composition	**Short- / long-term cyclability**	**Energy Density**	**Comments** (i.e. prolonged sintering, structures stability, etc.)
CMO	Excellent / Excellent	< 137 J/g	1. Prone to sintering 2. Transitions♣ reduce thermomechanical stability
CS5MO	Excellent / N/M	< 108 J/g	1. Prone to sintering 2. Sr-doping mitigates transitions♣ thus improves thermomechanical stability
CS10SMO	Excellent / N/M	< 99 J/g	1. Prone to sintering 2. High Sr-doping eliminates transitions♣ thus improves thermomechanical stability
CS10MF25O	Excellent / N/M	< 99 J/g	1. Prone to sintering

Composition		Short- / long-term cyclability	Energy Density	Comments (i.e. prolonged sintering, structures stability, etc.)
				2. High Sr-doping eliminates transitions♣ and substantially improves thermomechanical stability
Non-redox	A4	N/A	N/A	1. No sintering up to 1250°C 2. Challenges in materials pre-processing (difficult to mill/sieve) → potential difficulties in extrusion of "delicate" structures
	BM/B	N/A	N/A	
	T12	N/A	N/A	1. No sintering up to 1250°C 2. Finer particle size distribution.

♣: *Reversible structural transitions from orthorombic-to-cubic*

Table 2: Shortlisting of perovskites materials based on energy densities as measured from DSC measurements on powders and comments on their cyclability during 5 thermochemical cycles as well as on long-term cycling (>500 cycles) and comments on other potential important aspects for consideration in the project.

3. Manufacturing of small-scale structured specimens & characterization studies

The central idea of the project is to employ monolithic structured reactors/heat exchangers made entirely or partially of the redox oxide materials as the heat storage and thermal boosting medium. The concept is based on the inherent advantages of highly porous ceramic structures like monolithic honeycombs and reticulated foams vs. packed powder beds. These advantages include thin walls, high geometric surface area, good gas-solid contact, the ability to accommodate high gas flow rates with low pressure drop, ease of product separation and facile deposition of functional coatings.

These features, have led to the establishment of such "structured" catalytic systems, especially in the form of honeycombs, as the configuration of choice in a variety of catalytic applications, the most notable examples being automotive exhaust after-treatment and catalytic combustion [3]. Usually, such structured catalysts have large void fraction ranging from 0.7 to more than 0.9 (in the case of foams) compared to ca 0.5 in packed beds. Whereas honeycombs are the industrial configuration of choice being produced in millions of pieces annually, foams *"…exhibit extremely high porosities, that results in low pressure-drop, and with respect to their honeycomb monolithic counterparts, have a considerable degree of radial mixing, which is an advantage in processes limited by heat transfer*" [4]. Honeycombs are characterized by their cpsi (cells per square inch) number and foams by their ppi (pores per linear inch) number; Higher cpsi/ppi numbers mean "denser" structures with thinner channel walls/struts and more, but smaller, air flow channels per cross-section area unit, i.e. higher gas-solid contact area per unit volume.

The shaping routes for these two structures, even though different, share some common characteristics and steps. Both routes initially require a powder of fine size distribution with the mean diameter and a significant percentage of it to be less than 10 microns. Water and organics are added to the powder, in different quantities and for different purposes in each route, to enable and facilitate shaping into the final desired structure. After shaping, the structured "green" body is dried and then calcined and sintered so that first the water and the organics are removed and eventually the powder densifies and forms the rigid ceramic object.

3.1 Extruded honeycombs

Honeycombs are manufactured by extrusion: a small quantity of water is added to the powder, necessary so that the mixture forms a "stiff" paste, which then, by applying pressure, is forced to flow through a die to acquire the shape of the honeycomb. The preparation of small (laboratory) scale porous extruded honeycombs was carried out at CERTH with continuous consultation/guidance from LET, due to their extensive know-how in extrusion and powder shaping techniques in general. KB provided input on the handling and structuring of their raw materials (general recipe, binders, raw powders in quantities of 10-100 kg); namely compositions coded as A4, BM/B (see relevant details in Deliverable D2.4) and T12. Selected promising redox powders, as shortlisted by WP2 (see relevant details in deliverables D2.2 and D2.3), were synthesized and provided by WP2 as several batches in the range of 0.2–2 kg each.

The development work carried out by CERTH concerned the preparation of extrudable pastes for the production of mechanically robust cylindrical monolithic honeycombs with diameters in the range of 24–28 mm and adjustable lengths as required, but typically ~24 mm.

The main parameters influencing the quality of the small-scale extruded honeycombs produced are the following:

- The rheological properties of the extrusion paste, which are defined by the relative amounts of water, organic binder, the redox formulation and organic plasticizers.
- The drying process/protocol of the extruded honeycombs.
- The de-binding and sintering protocol of dried honeycombs (called green bodies)

Due to the public nature of the present deliverable, confidential details of the exact values and parametric analysis to define the above parameters in detail are not provided herein. The die geometries used for the extrusion tests are shown in Figure 3 (a and b).

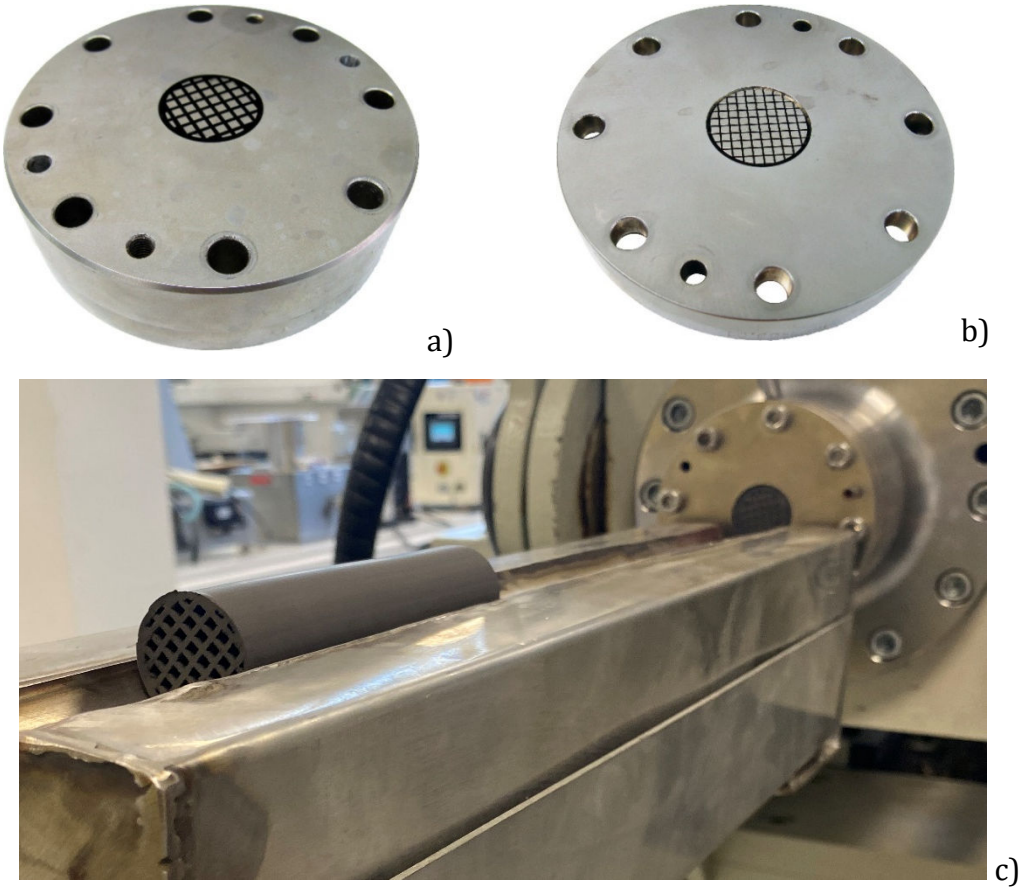

Figure 3: Photographs from ∅ 28mm extrusion dies used for the manufacturing of honeycombs from CMO-based powders and refractory industrial by-products: a), 44 cells per square inch (cpsi) and b) 90 cpsi, c) extrusion of CMO-based perovskite honeycombs.

The result was the successful extrusion of honeycomb geometries (Figure 4) using the two extrusion dies presented earlier, the first at 44cpsi, with thicker walls and the second one with thinner walls and higher cell density.

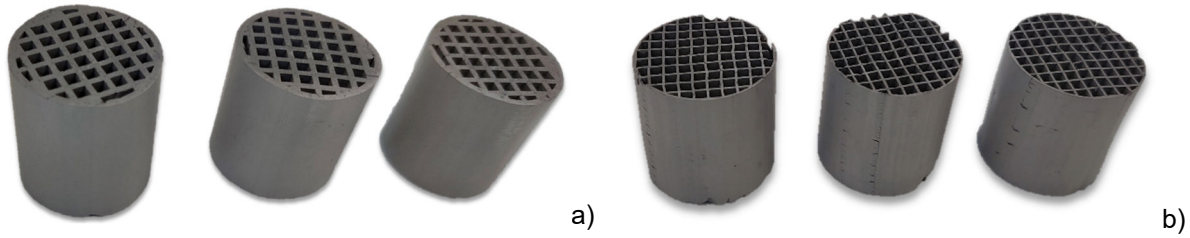

Figure 4: Photographs of extruded CMO structures calcined at 1300°C; The structures are derived from the use of: a) the 44 cpsi extrusion die, b) the 90 cpsi extrusion die.

The extrusion results were almost identical for two different redox formulations: a plain CMO (Figure 5a) and a Sr-doped CMO perovskite, CS10MO (Figure 5b). The powder for the latter extrusion, i.e. CS10MO (Figure 5b), was synthesized on a 2 kg scale and supplied by DLR for extrusion at CERTH.

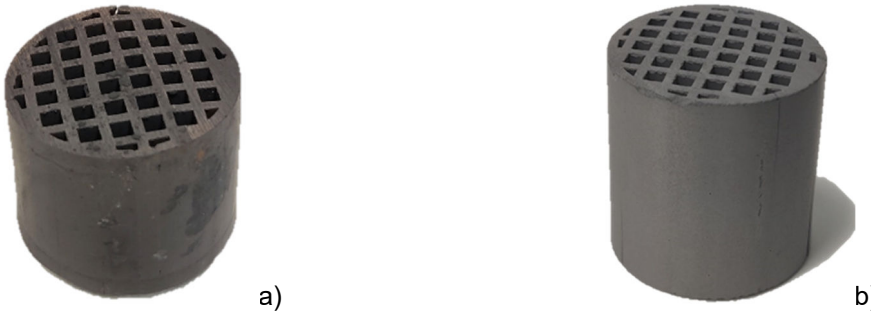

Figure 5: Photographs of extruded structures with the 44 cpsi die after calcination at 1300°C: a) CMO and b) Sr-doped CMO, i.e. CS10MO honeycombs.

The extrusion results obtained with the use of the three compositions provided by KB were similar (Figure 6).

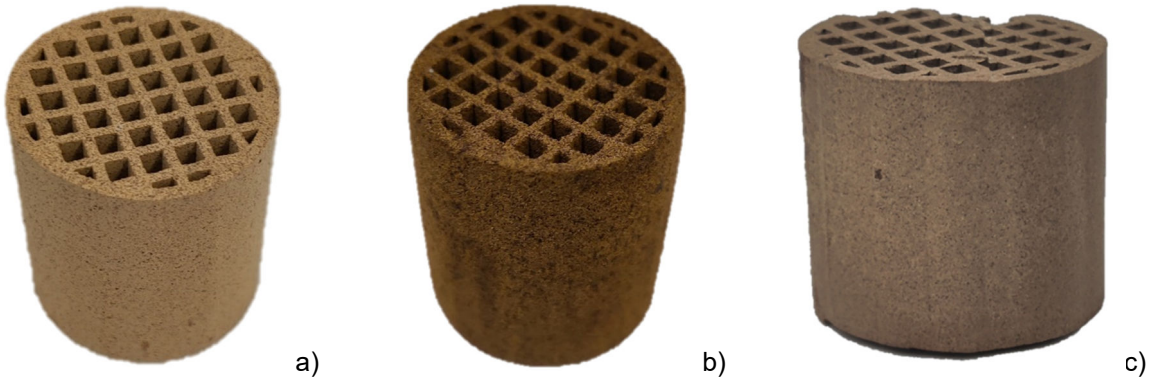

Figure 6: Photographs of extruded honeycombs by using of KB's compositions and the 44 cpsi extrusion die after sintering at 1250°C: a) A4, b) BM/B and c) T12.

It has to be mentioned that the honeycombs were produced with extrusion dies with nominal cell densities of 44 and 90 cpsi. However, after drying and calcination, due to the (expected) shrinkage of the ceramic pieces during sintering, the honeycombs finally produced exhibited higher cell densities (i.e. 59 and 111 cpsi respectively). Therefore, in the following text and figures such specimens are referred with either or both of these cpsi numbers (i.e. 44, 59 or 44/59).

3.2 Foam structures

DLR focused on the production of reticulated porous ceramics (RPCs), also known as "ceramic foams", via the process known as the polyurethane (PU) foam replica method. Water is also added to the perovskite powder, but in much higher quantities than in the extrusion process, to form a powder slurry. The procedure involves coating of "sacrificial" polyurethane (PU) foam templates (Figure 7a) with the slurry of the perovskite powder, removing excess slurry from the coated PU foams by "squeezing" or centrifugation, drying, and finally calcination for de-binding and sintering, where the original PU foam template is slowly burned out and the layers of the powder particles that are deposited on it sinter and form a ceramic "replica" of the original PU foam (Figure 7b). The characteristic microstructure of the ceramic product is shown in Figure 7c, where large quasi-spherical mega-pores are formed between an interconnected network of ceramic

"struts". The latter are usually hollow inside, exactly due to the "sacrificial PU template" which was occupying the now void/empty space. A wide variety of CMO-based foams ranging from 15-72 mm in diameter and 15-35 mm in height, in the 10-60 ppi range, have been produced (Figure 7b), in compliance with the space requirements/limitations of the test devices in which these foams were eventually scheduled to be tested.

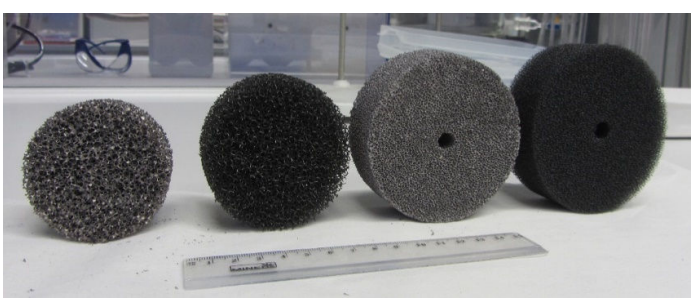

(a)

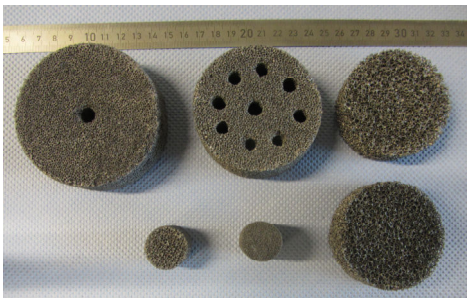

(b)

(c)

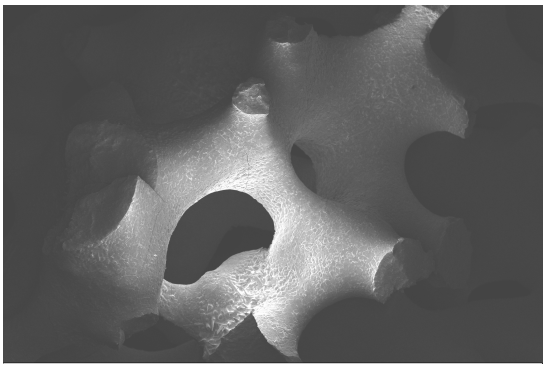

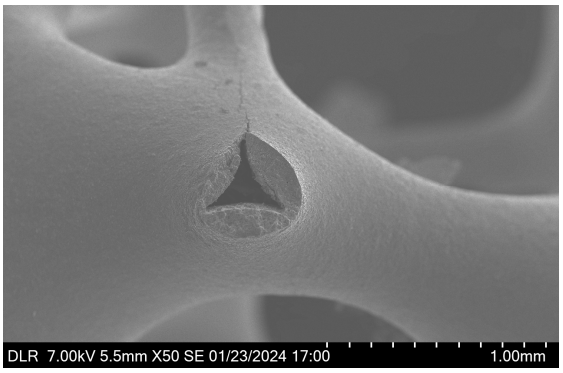

Figure 7: (a) Typical Ø 57 and Ø 72 mm sintered CS10MO foams vs. Ø 70 and Ø 80 mm PU templates used for their preparation (shrinkage due to sintering ~ 10-18.5 %, depending on template type and processing conditions); (b) various in-house manufactured foams of Ø 15-72 mm X 15-35 mm in height, with and without tailor-made perforation; (c) SEM photographs showing the microstructure of foams and the hollow character of the struts.

A graph showing the apparent viscosity of two CS10MO slurries of different solids content as a function of shear rate is shown in Figure 8. The high solids content is necessary so that to deposit on the PU template enough solid material, which upon subsequent sintering will form a well-connected and coherent solid ceramic struts network structure. Both slurries, even the one with the higher solids content, exhibit the desired shear thinning behaviour, i.e. their apparent viscosity decreases with increasing shear rate. This feature is necessary for handling of the slurries and for an efficient coating process; the slurry should become less and not more viscous under intense stirring for example, or when passing through narrow passages through the porous structure of the PU foams wherein the shear stresses developed are higher. Slurries of such solids content and of that rheological characteristics were ideal for coating PU foams of dimensions up to 80 mm so far.

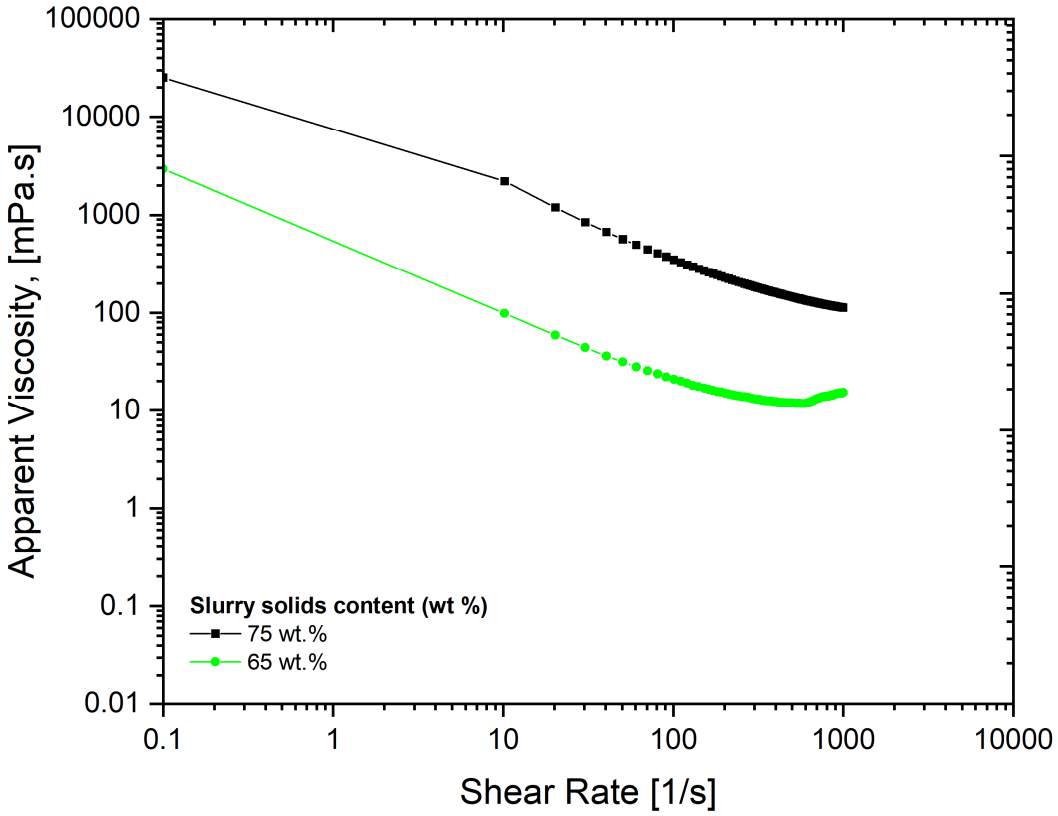

Figure 8: Shear-thinning behavior of typical CS10MO slurries used for the preparation of foams Apparent viscosity as a function of shear rate for two slurries of different solids content.

4. Macroscopic quality assessment of structured bodies & relevant measurements

4.1 Extruded honeycombs

The initial extrusion trials on CMO were carried out using the 44 cells per square inch (cpsi) die to investigate the feasibility of producing robust honeycomb structures. The trials were designed to assess the effect of various extrusion and sintering parameters on the mechanical integrity, dimensional stability and density of the honeycombs. In particular, the study focused on crack formation/growth during the removal of the organic components, i.e. calcination/sintering, the effect of sintering temperature on the final properties of the structures and the possible impact of parameters such as extrusion piston speed.

The first set of extrusion trials resulted in segments with significant cracking, particularly on the peripheral walls (see Figure 9). Despite these cracks in the green bodies, the structures retained their overall integrity after sintering with no further crack propagation. This resulted in mechanically stable bodies suitable for further evaluation.

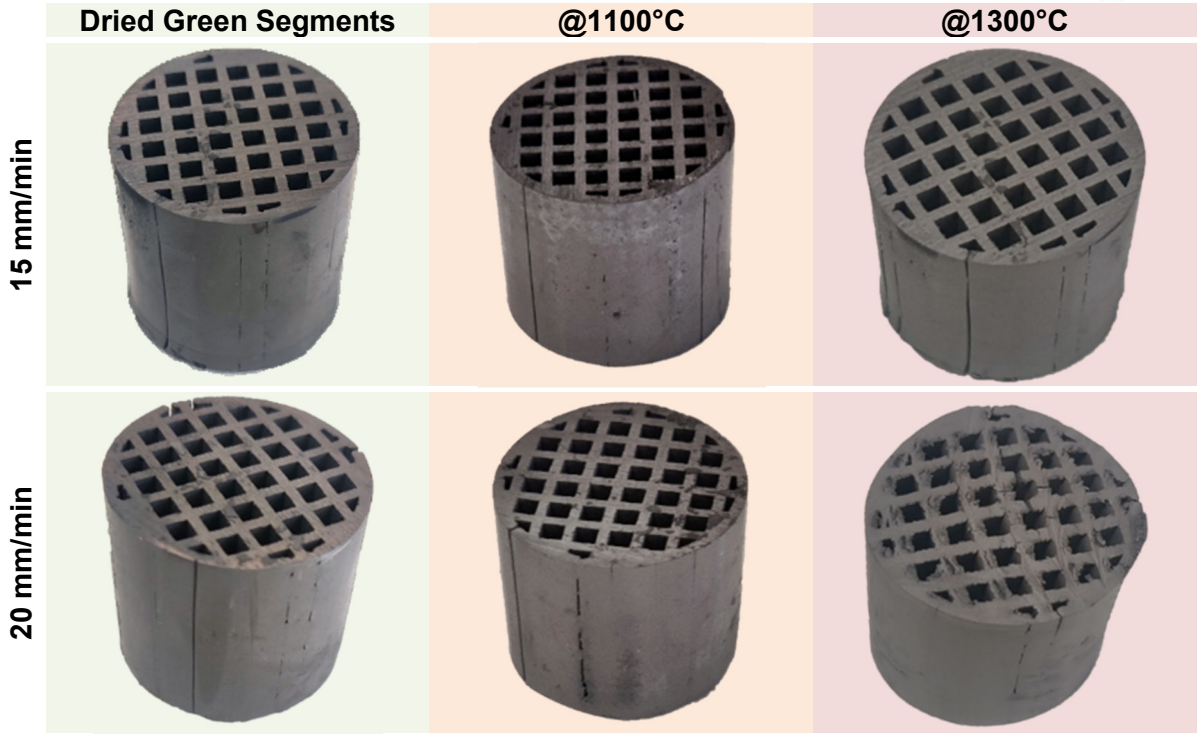

Figure 9: CMO monoliths prepared with two different piston speeds (15 mm/min and 20 mm/min) in their green state and after sintering at 1100°C and 1300°C.

Among the parameters evaluated during the extrusion trials, the speed of the extrusion piston was also studied (Figure 10). The graph correlates the extrusion piston speed with the (bulk) density of the segments. Normally for a given geometry, the bulk density is a first qualitative measure of the robustness of a structure; i.e. higher bulk density relates to more robust bodies. In addition to the density of the dried segments, the densities after sintering at two different temperatures are also shown, but the effect of the sintering temperature will be discussed in the following paragraphs. While no significant effect was observed with variations in piston speed, there was a slight trend indicating that an increase in extrusion speed could result in higher densities and thus more robust structures. This suggests that although extrusion speed does not have a profound effect, slightly higher speeds may improve the structural integrity and density of the extruded segments.

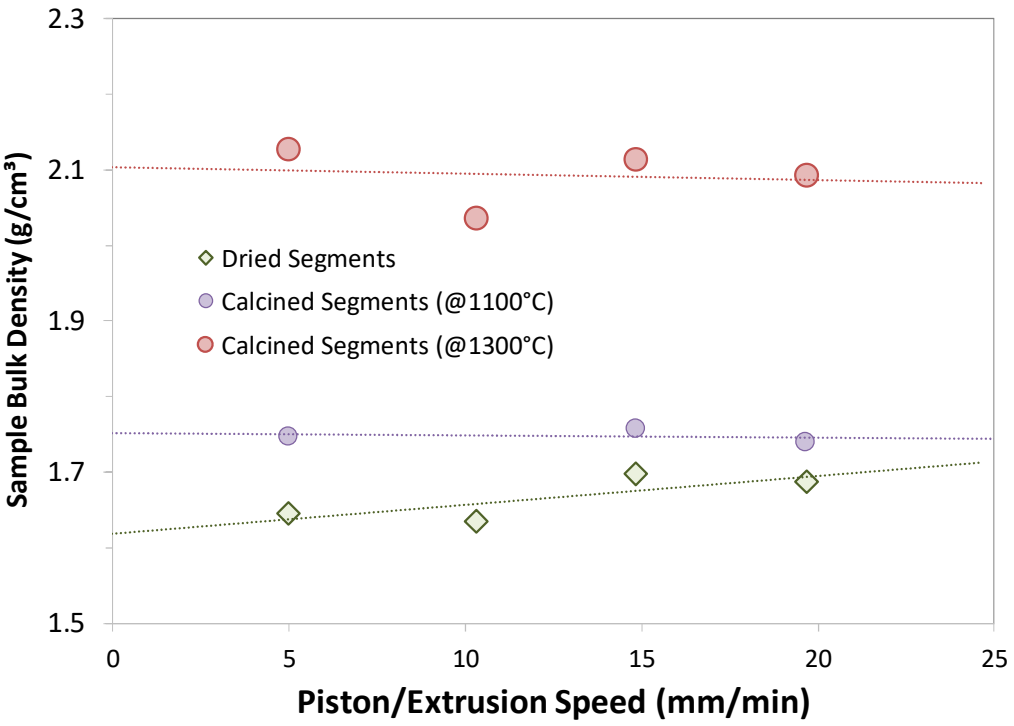

Figure 10: Comparative plot of the bulk density measured on CMO structures, as a function of extrusion piston speed when dry and after sintering at 1100°C and 1300°C.

Various calcination protocols in air were evaluated to facilitate the controlled removal of organic components (e.g. binders and plasticizers) from the green bodies while maintaining mechanical strength through controllable sintering of the structure. The calcination protocols used in the CMO segments resulted in effective removal of organic additives without causing excessive cracking or deformation, ensuring improved mechanical stability of the sintered structures. Figure 11 shows two of the calcination protocols applied, while Figure 9 visualizes the segments obtained after application of the specific sintering protocols. The first steps, i.e. the slow heating rates and the isothermal steps, <600°C, are aimed at removing the organic additives, while the increase in the maximum sintering temperature is aimed at increasing the robustness via controlled sintering.

As shown earlier in the graph of Figure 10 the sintering temperature had a profound effect on both the density and mechanical robustness of the segments. Higher sintering temperatures resulted in denser bodies (approximately +20%) with improved structural integrity, i.e. less fragile, which was obvious from macroscopic observation but not visible in the images provided (Figure 9). Specifically, sintering at 1300°C produced bodies with a density of 2.10 g/cm^3 compared to 1.75 g/cm^3 for those sintered at 1100°C. This suggests that higher sintering temperatures produce stronger and more robust structures.

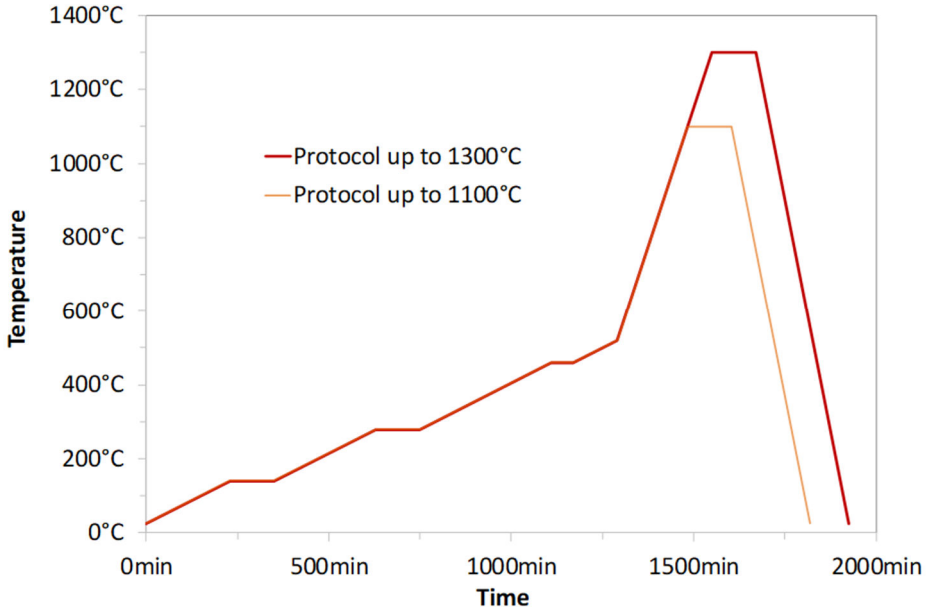

Figure 11: The two sintering profiles applied to CMO segments at 1100°C and 1300°C, showing the temperature progression during the entire sintering process.

Following the initial extrusion trials, adjustments were made to optimize the extrusion parameters. These improvements led to the production of flawless segments, with no cracks observed in the green bodies, thereby resolving the issues observed during the first set of trials. As demonstrated in Figure 12, the subsequent sintering process resulted in equally flawless segments. As previously noted, the sintered segments exhibited enhanced mechanical stability.

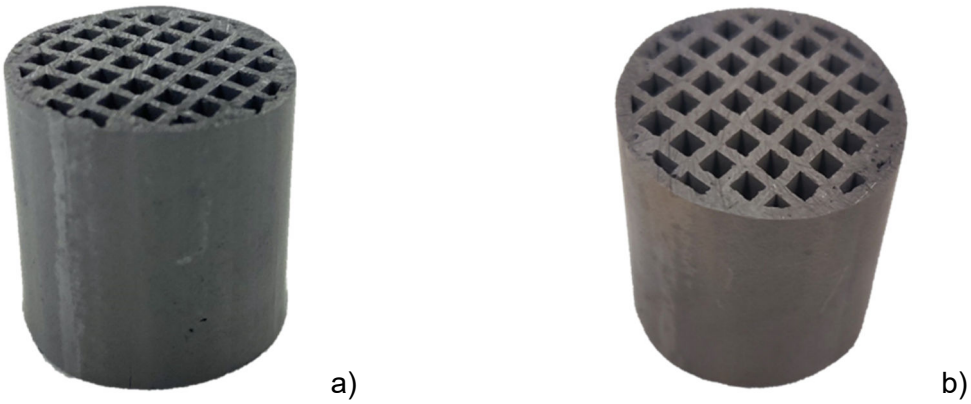

Figure 12: Photographs of a) a dried CMO monolith (44 cpsi) and b) the same monolith after sintering at 1300°C.

The next step was to apply the optimized extrusion procedure to extrude monoliths of higher cell densities, i.e. use of the 90 cpsi die. As outlined in Section 2.1, these higher-density monoliths featured thinner and more delicate walls, as depicted in Figure 4. Despite the increased complexity and thinner walls of these structures, the optimized extrusion process still resulted in monoliths that were free of any major defects. The 44cpsi geometry offers a more robust structure than the 90 cpsi one, while also

demonstrating higher densities. This means a greater amount of active material per reactor volume. This increased density could translate to higher performance per unit reactor volume, providing a significant advantage for applications requiring high efficiency and stability. In addition, it reinforces their potential for industrial-scale applications.

Given the success of the 44cpsi geometry in producing robust and high-density structures, the remaining materials under investigation were extruded using the aforementioned die. These included the Sr-doped CMO powder provided by DLR (CS10MO monolith shown in Figure 5) and three KB powders (monoliths shown in Figure 6). Use of the same extrusion die allowed for consistent comparison across different materials and cell densities.

As shown in Table 3, the dimensional changes observed during the sintering of all extruded honeycombs are summarized. While it is generally accepted that sintering leads to shrinkage, this was not the case for the two KB powders, A4 and BM/B. Expansion was recorded for these two powders, which ultimately led to lower densities for the sintered bodies. The third KB powder, T12, did not exhibit any expansion. However, the organic content of T12 resulted in the preservation of its initial density after sintering.

	Die used (cpsi)	Diameter		Length % Change	Bulk Density	
		(mm)	% Change		(g/cm³)	% Change
CMO	90	25.90	-8.16%	-7.57%	1.20	22.5 %
CMO	44	26.30	-7.72%	-7.01%	2.08	20.2 %
CS10MO	44	25.79	-8.60%	-8.55%	2.25	24.7 %
A4	44	29.01	3.28%	+2.79%	1.20	-17.8 %
BM/B	44	29.68	4.95%	+4.70%	1.00	-21.3%
T12	44	24.68	-6.82%	-4.47%	1.45	2.30 %

Table 3: Dimensional changes recorded during sintering of honeycombs extruded at CERTH.

The porosity values and median pore diameters of pristine monoliths extruded at CERTH are compared in Figure 13. For the same chemical composition (CMO), the geometry of the die does not have a significant effect on either the porosity or the median pore diameter. Doping with 10% Sr also has a minimal effect: the doped monolith has a porosity of 24.6% and a mean pore diameter of 1.12 μm, compared to 27% porosity and 1.36 μm for the undoped monolith. In contrast, with porosities ranging from 26.1% to 50.1% and median pore diameters ranging from 1.41 μm to 46 μm, the monoliths prepared from the three KB powders show a wider range. The BM/B sample has the highest porosity and the highest median pore diameter, while the T12 sample produces structures that are similar to those produced with perovskites, and the A4 sample lies in between.

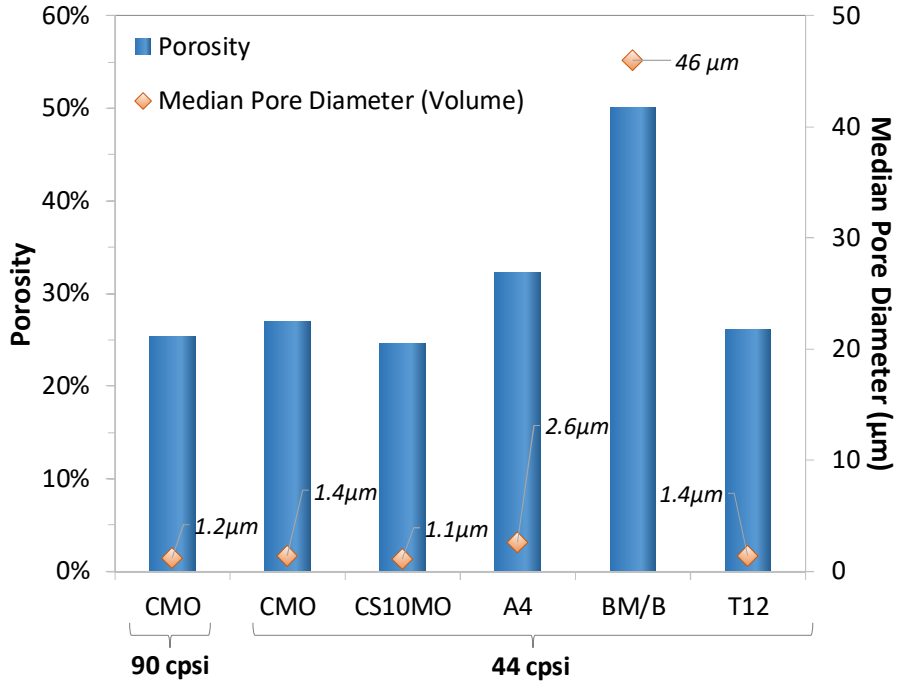

Figure 13: Comparative porosity values and median pore diameters values of pristine monoliths extruded at CERTH.

The optimized extrusion procedure demonstrated the feasibility of producing monoliths with minimal defects and various cell densities/die geometries. Between the two evaluated structures, the robust nature of the 44cpsi geometry, combined with its higher density, makes it a favorable option for high-performance applications. Furthermore, the findings of the sintering trials for the various materials under investigation highlight the necessity of considering both the material composition and the extrusion die choice, as they can significantly influence the final properties of the honeycomb structures.

4.2 Foam structures

The slurry-coated PU templates were dried at ambient temperature overnight, placed on alumina tiles and fired. Similarly to the case of honeycombs, various calcination protocols in air were also tested in order to produce rigid, ceramic foam pieces. It has to be noted though that in the case of foams, the whole PU template has to be removed by burn-out and not just the organic additives in the slurry. Since the PU structure is the one that initially "supports" the ceramic powder deposited on it, its removal has to be performed in a controlled manner and very slowly, so that the ceramic structure does not collapse; the subsequent stages of sintering have to induce mechanical strength on the structure. Figure 14 shows two of the calcination protocols applied with maximum sintering temperatures of 1200 and 1300°C. Specimens sintered at both these temperatures were rigid enough to be further handled. The much longer time vs. the honeycombs case is due to the very low heating rate employed due to the issues relevant

to the PU template and the much more "open" with respect to honeycombs, foam structure, mentioned above.

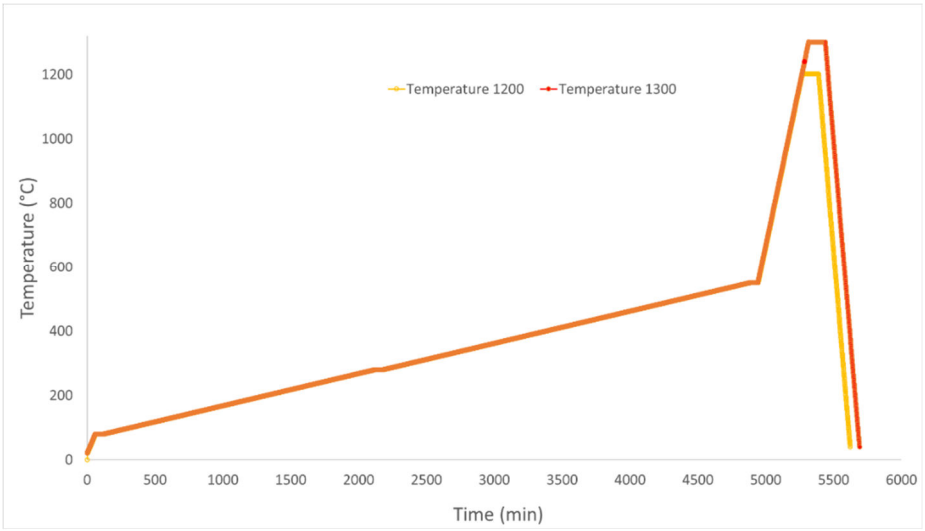

Figure 14: Two sintering profiles applied to CMO-based foams with sintering temperatures of 1200°C and 1300°C, showing the temperature progression during the entire sintering process.

Table 4 provides the shrinkages and bulk densities of representative manufactured foam porous structures of ~ Ø 25 mm. The lower bulk densities of the foams vs. those of the honeycombs listed in Table 3, are evident.

Composition/Sintering temperature	CMO 1200°C		CS5MO 1200°C		CS10MO			
					1200°C		1300°C	
ppi	30	60	30	60	30	60	30	60
Diameter (mm)	25.5	25.5	25.9	25.5	25.5	26.0	24.5	24.9
Diameter % change	-5.51	-5.44	-4.18	-5.62	-5.55	-3.70	-9.18	-7.77
Length % change	-1.51	-4.55	-1.66	-4.81	-2.03	-3.44	-4.92	-6.94
Bulk density (g/cm^3)	0.74	0.81	0.76	0.80	0.68	0.71	0.74	0.80

Table 4: Dimensional changes recorded during sintering and resulting bulk densities of foams manufactured at DLR.

4.3 Porous structure characterisation by mercury (Hg) porosimetry

The porosity and pore size distribution of representative redox-active honeycombs (in-house made by CERTH) and foams (in-house made by DLR), redox-inactive honeycombs out of recycled materials from KB (in-house made by CERTH) and of commercial cordierite honeycombs are shown in Figure 15, Figure 16, Figure 17 and Figure 18 respectively. The values for the redox-active structures, honeycombs and foams, are summarized in Table 5 and Table 6 respectively.

The three in-house extruded redox honeycomb specimens, sintered at the same temperature of 1300°C (Figure 15) have very similar values of porosity and mean pore diameter, irrespective of differences in compositions or cpsi. Furthermore, they all exhibit a mono-modal, very narrow pore size distribution around the median.

Sintering temperature is also the main factor affecting the porosity of CS10MO redox foams (Figure 16); the higher the sintering temperature the lower the porosity. All foams exhibit a quasi-tri-modal pore size distribution curve with a "major" peak in the range 1-10 microns and two other, smaller peaks at higher mean pore diameters. Scheduled additional measurements for foams of 60 ppi made of all three compositions CMO, CS5MO and CS10MO will help in clarifying any effect of ppi and phase composition on porosity.

The non-redox honeycombs exhibit significant differences with respect to porous structure characteristics (Figure 17). Sample T12 that exhibited shrinkage has the lowest porosity and a monomodal pore size distribution of small pores around the median of 1.4 microns. The two samples that expanded upon sintering exhibit higher porosities, yet different characteristics. The pore size distribution curve of BM/B is very similar to that of T12, but shifted to much higher values of porosity and mean pore diameter. Sample A4 exhibits intermediate porosity and a tri-modal pore size distribution curve resulting in an intermediate value of the mean pore diameter as well.

Finally, with respect to commercial cordierite specimens (Figure 18), the porosity decreases with increasing channel density (cpsi). Furthermore, the ones of 400 and 600 cpsi have very similar pore size distribution curves, whereas the "denser" structure of 900 cpsi has a much narrower pores size distribution and lower median value.

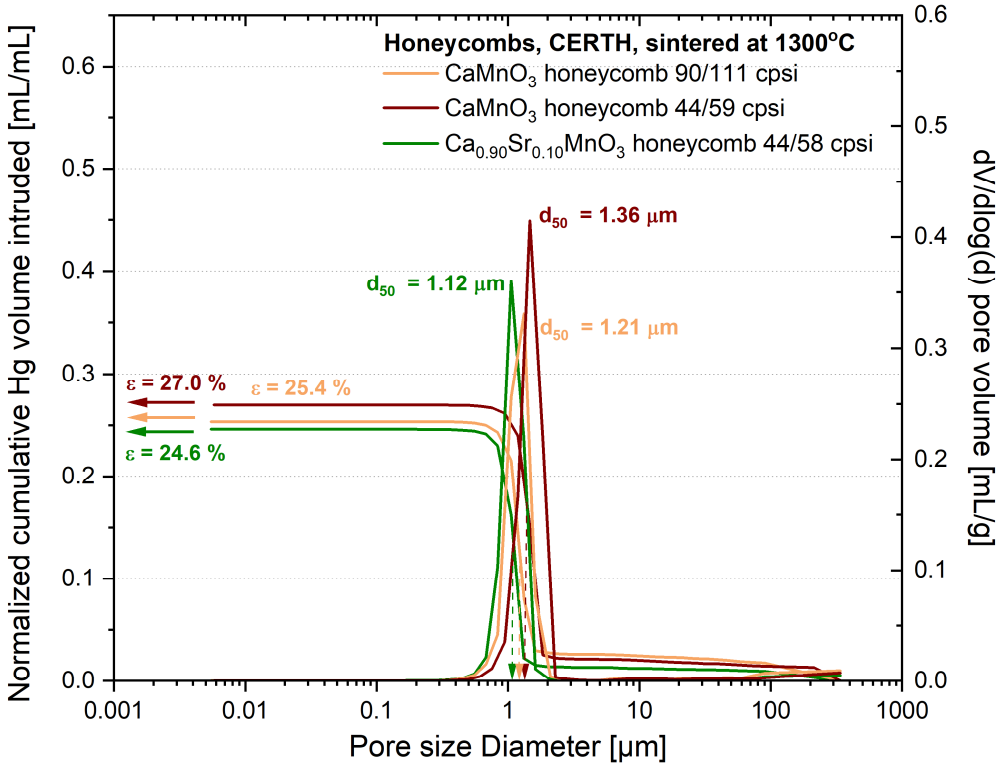

Figure 15: Porosity and pore size distribution of CMO-based perovskite honeycombs manufactured in-house by CERTH.

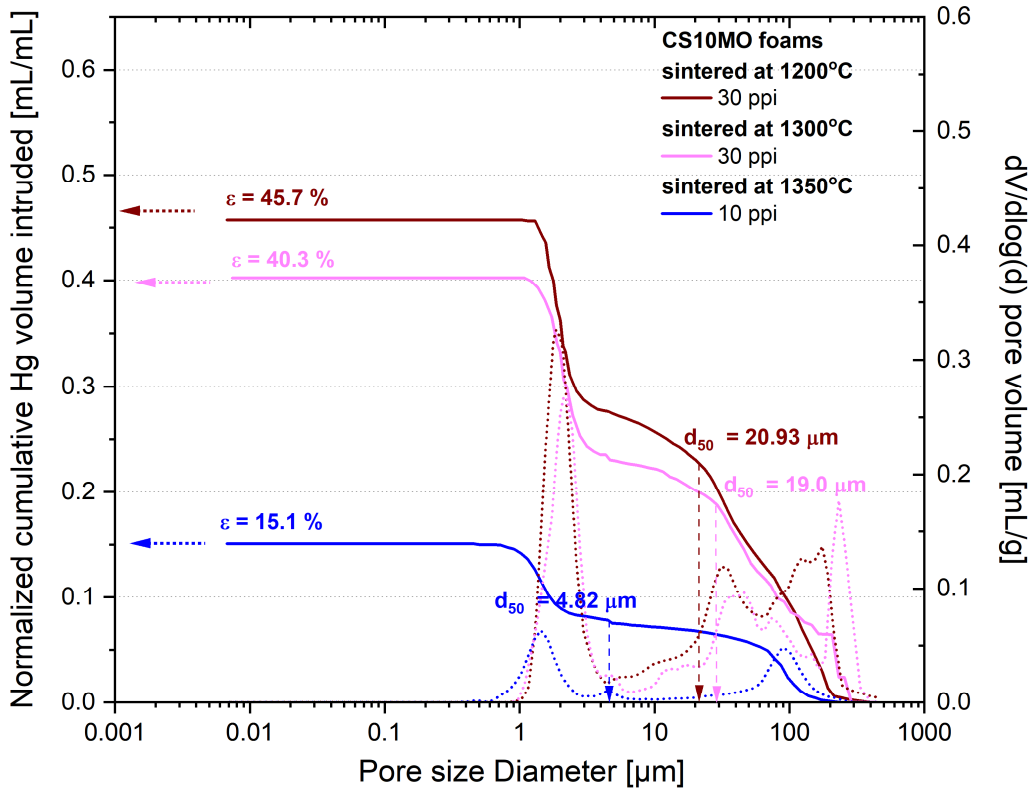

Figure 16: Porosity and pore size distribution of CMO-based perovskite foams manufactured in-house by DLR.

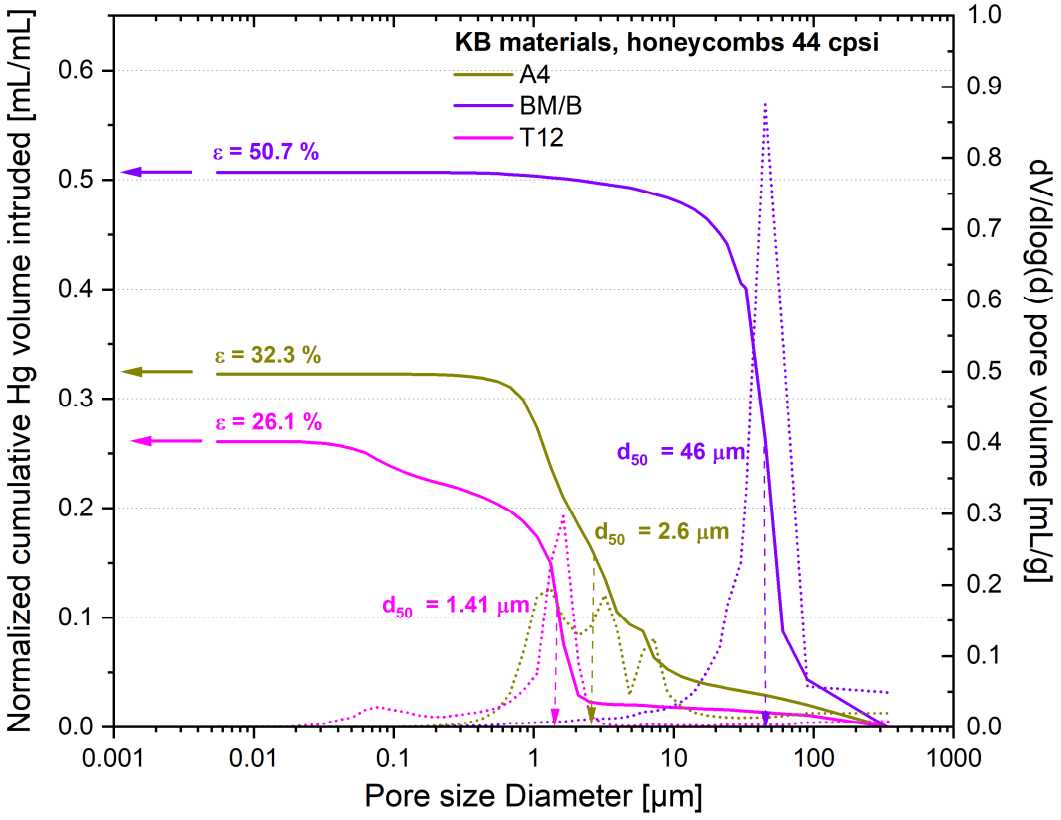

Figure 17: Porosity and pore size distribution of redox-inactive honeycombs manufactured in-house by CERTH from recycled materials supplied from KB.

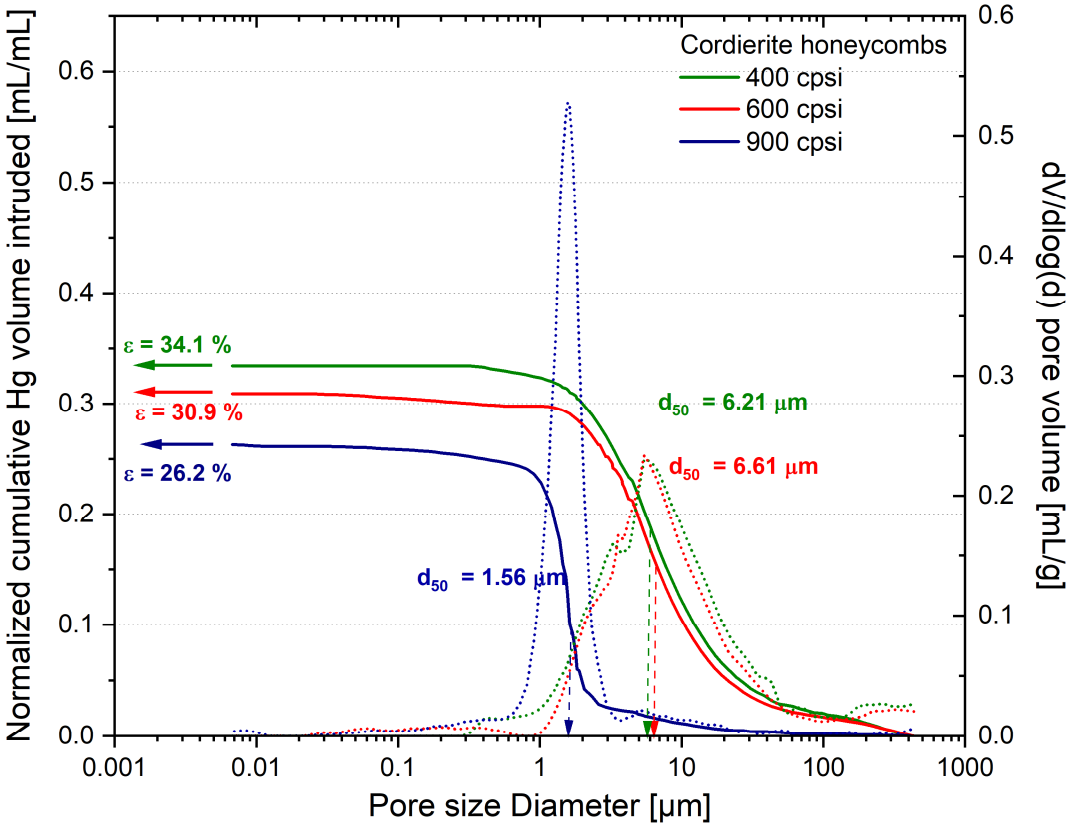

Figure 18: Porosity and pore size distribution of commercial cordierite honeycombs.

	CMO	CMO	CS10MO	A4	BM/B	T12
Die used (cpsi)	90	44	44	44	44	44
Porosity (%)	25.4	27.0	24.6	32.3	50.1	26.1
Median pore diameter (µm)	1.21	1.36	1.12	2.63	46.0	1.41

Table 5: Porosity values and median pore diameters of monoliths extruded at CERTH.

Composition	**CS10MO**		
Sintering temperature	**1200 °C**	**1300 °C**	**1350 °C**
ppi	**30**	**30**	**10**
Porosity (%)	45.7	40.3	15.1
Median pore diameter (µm)	20.9	19.0	4.8

Table 6: Porosity values and median pore diameters of foams manufactured at DLR.

5. Parametric studies and first redox assessment

5.1 Redox thermochemical performance vs. the respective redox powder formulations and Effect of calcination temperature

Deliverable D3.1 presents only indicative TGA/DSC results[1] of the redox structures, providing an indication of their redox activity. A more detailed performance evaluation of the structures has already been presented in Deliverable D3.2. The TGA data shown in Figure 19 compare a CMO powder with two CMO monolithic structures that after shaping were sintered at 1100°C and 1300°C. The weight changes recorded during a thermochemical protocol called "conventional"[2], are comparable for all the samples. Regarding the energy recorded with DSC, during isothermal oxidation at five different temperatures (namely 650°C, 700°C, 750°C, 800°C and 850°C, the second protocol used, also described in D2.3), higher sintering temperatures result in higher energy values compared to the 1100°C sample, although still lower than those observed for powder. The segment sintered at 1300°C exhibits repeatable and stable redox performance.

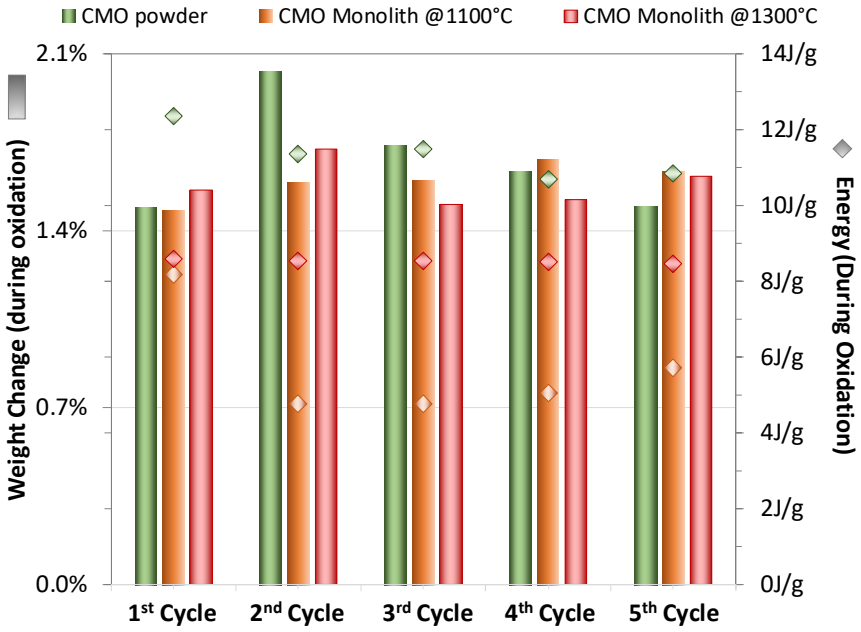

Figure 19: TGA results comparing a CMO powder with two CMO structures sintered at 1100°C and 1300°C. The weight changes are derived from a protocol in which the oxidation takes place during cooling from 1100 to 300°C, while the energy values for each of the five cycles are calculated during the isothermal oxidation of the segments at 650°C, 700°C, 750°C, 800°C and 850°C respectively.

1 Simultaneous Thermogravimetric (TGA) and Differential Scanning Calorimetry (DSC) Analysis.

2 The temperature profile and conditions applied during the thermochemical evaluation by TGA/DSC are described in detail in deliverable D2.3. In the "conventional" evaluation, the oxidation of the perovskite takes place during its dynamic cooling.

Similarly to the previous comparison, in Figure 20 the CMO powder is compared, this time with two Sr-doped CMO powders that have been thermally treated at 1200°C and 1300°C, respectively. The comparison shows the effect of Sr-doping on the redox behavior, which, as expected, leads to a reduction in the non-stoichiometric parameter (δ) calculated from the weight changes recorded with the conventional TGA protocol (same conditions as in Figure 19, where oxidation occurs during cooling). This reduction in δ indicates a slight decrease in redox activity with respect to the undoped CMO powder. The energy density recorded from DSC, follows a similar trend, showing a reduction with Sr doping. However, an interesting observation, for the Sr-doped powder treated at a lower temperature, i.e. 1200°C, is that the energy density remains relatively stable over all five oxidation temperatures (650°C, 700°C, 750°C, 800°C and 850°C), with a slight tendency to decrease with increasing oxidation temperature. On the other hand, the sample treated at 1300°C, while in the first cycle is showing extremely low values, it shows a significant recovery of the energy density after 5 thermochemical cycles. These results suggest that Sr doping and sintering temperature play an important role in controlling the redox performance and stability of the materials.

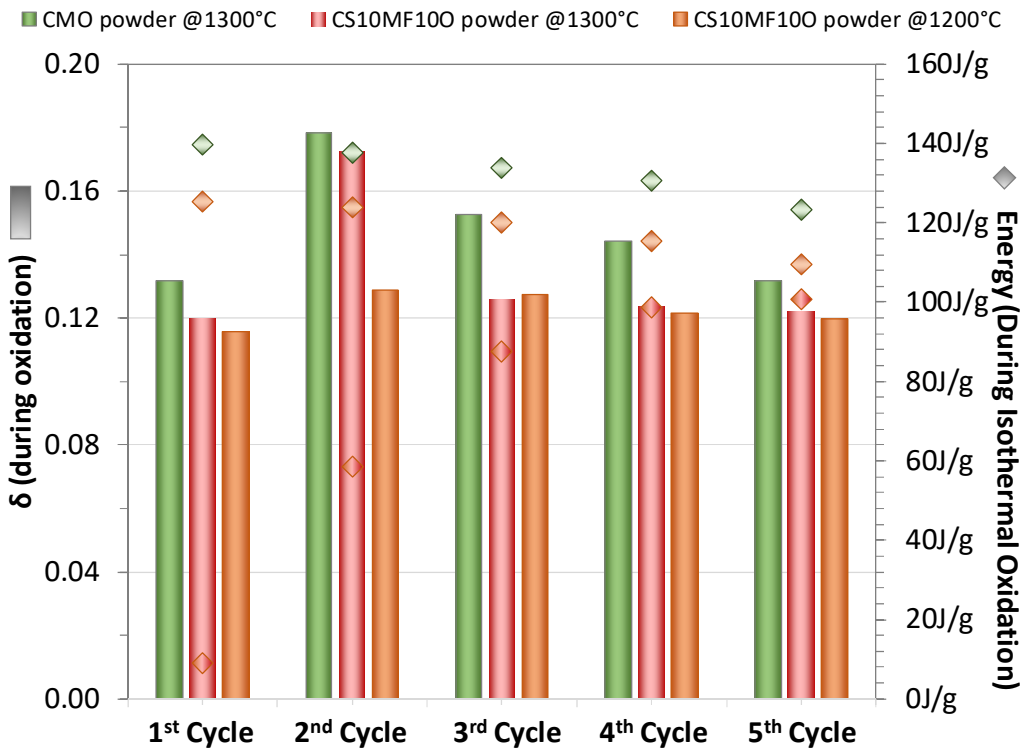

Figure 20: TGA/DSC results comparing a CMO powder with two Sr-doped CMO powders treated sintered at 1200°C and 1300°C. δ, is calculated from the weight changes recorded during the protocol in which oxidation takes place during cooling from 1100 to 300°C. The energy values for each of the five cycles are calculated during isothermal oxidation of the segments at 650°C, 700°C, 750°C, 800°C and 850°C respectively.

6. Conclusions

Lab-scale model specimens from both CMO-based compositions and redox inactive sensible-only materials sourced from steel-industry by-products (provided by KB) have been successfully prepared and characterized. Two methods were followed: the PU-sacrificial template method and piston extrusion. The main conditions and parameters of the two shaping methods are also reported herein but certain details are not disclosed due to the public nature of the deliverable. The measured properties of these structures indicate products of acceptable quality and their preliminarily assessed redox performance was similar to that of powders of the same compositions. Additional results complementing the work reported here and completing the necessary outcome of WP3 to be fed into WPs 4-6 are included in Deliverables D3.2 and D3.3.

7. References

[1] M. Pein, L. Matzel, L. de Oliveira, G. Alkan, A. Francke, P. Mechnich, C. Agrafiotis, M. Roeb, C. Sattler, Reticulated porous perovskite structures for thermochemical solar energy storage, Advanced Energy Materials, 12(10), 2102882, (2022).

[2] L. Klaas, M. Pein, P. Mechnich, A. Francke, D. Giasafaki, D. Kriechbaumer, C. Agrafiotis, M. Roeb, C. Sattler, Controlling thermal expansion and phase transitions in $Ca_{1-x}Sr_xMnO_3$ by Sr-content, Physical Chemistry Chemical Physics, 24, 27976-27988, (2022).

[3] D.M. Beall and W.A. Cutler, Smog begone! How development of ceramic automotive catalytic substrates and filters helped reduce air pollution, American Ceramic Society Bulletin, 99(3), 24-31, (2020).

[4] M.V. Twigg and J.T. Richardson, Fundamentals and Applications of Structured Ceramic Foam Catalysts, Industrial Engineering Chemistry Research, 46, 4166-4177, (2007).